Local Analysis of Shock Capturing Using Discontinuous Galerkin Methodology

H. L. Atkins*
NASA Langley Research Center
Hampton, VA 23681-0001

Abstract

The compact form of the discontinuous Galerkin method allows for a detailed local analysis of the method in the neighborhood of the shock for a nonlinear model problem. Insight gained from the analysis leads to new flux formulas that are stable and that preserve the compactness of the method. Although developed for a model equation, the flux formulas are applicable to systems such as the Euler equations. This article presents the analysis for methods with a degree up to 5. The analysis is accompanied by supporting numerical experiments using Burgers' equation and the Euler equations.

Introduction

The discontinuous Galerkin method is being developed as a means for obtaining a high-order shock capturing-capability on unstructured meshes. This capability is an important step toward achieving an efficient and robust method for aeroacoustic applications. The objective of this work is to determine whether a local eigenvalue analysis can predict the instabilities that have been previously observed, and to use insight gained from the analysis to suggests ways to eliminate the instability.

In reference 1, the discontinuous Galerkin method was formulated in a quadrature-free form that reduced both the computational effort and storage requirements. Reference 2 described the implementation of boundary conditions, including the treatment of curved walls and nonreflecting boundary conditions. In these works, the method was described in detail, and numerical results for scalar advection and for the Euler equations were shown to demonstrate the accuracy and robustness of the method. These studies showed numerically[1] that piecewise linear and piecewise quadratic discontinuous Galerkin methods were stable without the use of either limiters or added dissipation when applied to the nonlinear Burgers' equation for a shocked case. However, higher order methods diverged immediately after shock formation. Also in reference 1, it was observed in numerical test that the quadratic form was stable only if the flux integral term was evaluated exactly.

The discontinuous Galerkin has a number of fundamental properties essential to any robust shock capturing method. In a series of papers, Cockburn and Shu[3] and Cockburn et al.[4, 5] discussed the discontinuous Galerkin method with the use of approximate Riemann solvers, limiters, and total-variation-diminishing (TVD) Runge-Kutta time discretizations for nonlinear hyperbolic problems. Reference 5 presents the design of a limiter that applies to general triangulations, maintains a high order of accuracy in smooth regions, and guarantees maximum norm stability. Jiang and Shu[6] also proved that the discontinuous Galerkin method satisfies a local cell entropy inequality for the square entropy $\eta(U) = U^2$, for arbitrary triangulations in any space dimension, and for any order of accuracy. This proof trivially implies the L_2 stability of the method for nonlinear shocked problems in the scalar case.

Flux limiting has been demonstrated as a means for stabilizing the shocked case;[5, 7] however, this approach tends to reduce the formal accuracy and to diminish the compactness of the method. This work presents a local eigenvalue analysis that predicts the stability, or instability, of the method for the Burgers' equation when a shock is present. The analysis is possible only because of the compact nature of the discontinuous Galerkin method. The analysis also provides physical insight into possible causes of the instability and leads to flux formulas that eliminate the instability.

The first section describes the discontinuous Galerkin method applied to the nonlinear Burgers' equation and provides the rationale for the analysis. The second section describes in detail the analysis and the conclusions drawn from it. The third sec-

* Senior member, AIAA

tion presents numerical experiments with the new flux function using the scalar Burgers' equation. The last section presents numerical experiments with the Euler equations.

Discontinuous Galerkin Method

Application of the semidiscrete form of the discontinuous Galerkin method to the scalar hyperbolic equation of the form

$$\frac{\partial U}{\partial t} + \frac{\partial F(U)}{\partial x} = 0 \qquad (0 < x < 1,\ t > 0) \qquad (1)$$

begins by partitioning the domain into nonoverlapping elements that cover the domain: $0 = x_0 < \ldots < x_i < x_{i+1} < \ldots < 1$. Within each element, the solution is approximated by a subspace that is defined local to the element. In the present work, the subspace will be the set of polynomials of degree $\leq n$: $\mathcal{S} = \{1, \xi, \xi^2, \ldots, \xi^n\}$. Within each element, $x = \bar{x}_i + \triangle x_i\ \xi$, $\bar{x}_i = (x_{i-1} + x_i)/2$, and $\triangle x_i = x_i - x_{i-1}$. The solution in element i is approximated by

$$U(x,t) \approx V_i(\xi,t) = \sum_{j=0}^{n} v_{i,j}(t)\xi^j$$

for $x_{i-1} < x < x_i$.

The evolution of the dependent variables $v_{i,j}(t)$ is governed by the projection of equation (1) onto the same subspace that is used to approximate the solution:

$$\int_{-\frac{1}{2}}^{\frac{1}{2}} \xi^j \left(\frac{\partial V_i}{\partial t} + \frac{\partial F(V_i)}{\partial x} \right) d\xi = 0 \qquad (0 \leq j \leq n)$$

Integration by parts yields the weak conservation form of the equation, which is used in the numerical solution:

$$\int_{-\frac{1}{2}}^{\frac{1}{2}} \xi^j \frac{\partial V_i}{\partial t}\, d\xi + \triangle x_i^{-1} \left[- \int_{-\frac{1}{2}}^{\frac{1}{2}} j\xi^{j-1} F(V_i)\, d\xi + (\tfrac{1}{2})^j \widehat{F}(x_i) - (-\tfrac{1}{2})^j \widehat{F}(x_{i-1}) \right] = 0 \qquad (2)$$

or

$$\mathcal{L}_j \cdot V_i(\xi) + \triangle x_i^{-1} \left[(\tfrac{1}{2})^j \widehat{F}(x_i) - (-\tfrac{1}{2})^j \widehat{F}(x_{i-1}) \right] = 0 \qquad (3)$$

for $j = 0,\ 1,\ 2,\ \ldots,\ n$.

The $\mathcal{L}_j \cdot V_i(\xi)$ term, which contains the two integral terms of equation (2), depends only on the solution within the element. In the quadrature-free form,[1] the flux is approximated as a polynomial in ξ, and the second integral is evaluated exactly. Formal error convergence properties are obtained in smooth regions with the flux truncated to a polynomial of degree $n+1$. For nonlinear problems with shocks, stable solutions of the quadratic case ($n = 2$) were obtained only when the flux was evaluated exactly.

At the element boundaries, where the solution is not unique, the $\widehat{F}$ terms are evaluated based on the solution that is "upwind" (in the sense of characteristic directions) of the element boundary. $\widehat{F}$ is generally written in the form of a Riemann flux as $\widehat{F}(x_i) \equiv \mathcal{F}^R(U_L, U_R)$, where U_L and U_R denote solutions from the left and right sides of the element boundary, respectively. Hence, adjacent elements communicate with one another only through $\widehat{F}$. As a consequence, each element can be thought of as a somewhat autonomous entity that responds to inflow boundary conditions provided by the element(s) "upwind" of itself.

Elements Near a Shock

Under somewhat idealized conditions, the stability of the overall solution depends heavily, if not entirely, on the behavior of the method in the element that contains the shock. To show this, consider the model problem in which $F(U) = \frac{1}{2}U^2$ and equation (1) is supplemented with the following initial and boundary conditions:

$$U(0,t) = -U(1,t) = 1$$

$$U(x,0) = \begin{cases} 1 & x < X_s \\ -1 & x > X_s \end{cases}$$

The approximate Riemann flux commonly used with this model problem is of the form

$$\mathcal{F}^R(U_L, U_R) = [F(U_R) + F(U_L) - \lambda(U_R - U_L)]/2$$

where $\lambda \geq |U_R + U_L|/2$. If $\lambda = |U_R + U_L|/2$, then this flux is an exact splitting

$$\mathcal{F}^R(U_L, U_R) = \begin{cases} F(U_L) & \text{if } \lambda > 0 \\ F(U_R) & \text{if } \lambda < 0 \end{cases}$$

and also has the following property commonly associated with Roe's flux :[4]

$$\lambda\,(U_R - U_L) = \pm\,[F(U_R) - F(U_L)]\,.$$

Next, assume that an exact discrete solution exists and that the solution is sufficiently accurate such that the sign of λ for the discrete solution is the same as the sign of the exact solution (i.e., $\text{sign}(U) = \text{sign}(\lambda)$). Also let I denote the index of the element within which the shock lies (i.e., $x_{I-1} < X_s < x_I$).

Then for all element boundaries to the left of element I, $\lambda > 0$ and $\widehat{F}(x_i) = F(V_i(\frac{1}{2}))$. Similarly, for all element boundaries to the right of element I, $\lambda < 0$ and $\widehat{F}(x_i) = F(V_{i+1}(-\frac{1}{2}))$. Hence, equation (3) becomes

$$\begin{aligned} \mathcal{L}_j \cdot V_i &+ \triangle x_i^{-1} (\tfrac{1}{2})^j F(V_i(\tfrac{1}{2})) \\ &= \triangle x_i^{-1} (-\tfrac{1}{2})^j F(V_{i-1}(\tfrac{1}{2})) \quad (i < I) \end{aligned} \tag{4}$$

$$\begin{aligned} \mathcal{L}_j \cdot V_i &= -\triangle x_i^{-1} \left[(\tfrac{1}{2})^j F(V_{i+1}(-\tfrac{1}{2})) \right. \\ &\quad \left. -(-\tfrac{1}{2})^j F(V_{i-1}(\tfrac{1}{2})) \right] \quad (i = I) \end{aligned} \tag{5}$$

$$\begin{aligned} \mathcal{L}_j \cdot V_i &- \triangle x_i^{-1} (\tfrac{1}{2})^j F(V_i(-\tfrac{1}{2})) \\ &= -\triangle x_i^{-1} (-\tfrac{1}{2})^j F(V_{i+1}(-\tfrac{1}{2})) \quad (i > I) \end{aligned} \tag{6}$$

When considered separately, the subdomains to the left and to the right of element I, which are governed by equations (4) and (6), respectively, are stable and well behaved (and trivially satisfied by the initial conditions). Hence, all elements to the left and to the right of element I can be thought of as simply supplying boundary conditions to element I. Thus, the stability of the overall problem is contingent on the existence and stability of the solution within the element that contains the shock.

Analysis of Shock Containing Element

Motivated by the previous discussion, we consider the behavior of equation (5), in which the approximate Riemann flux terms $\widehat{F}$ are evaluated at the state specified by the boundary conditions (the element subscript has been dropped for clarity):

$$\begin{aligned} &\int_{-\frac{1}{2}}^{\frac{1}{2}} \xi^j \frac{\partial V}{\partial t} \, d\xi - \triangle x^{-1} \int_{-\frac{1}{2}}^{\frac{1}{2}} j\xi^{j-1} F(V) \, d\xi \\ &\quad = -\triangle x^{-1} \left[(\tfrac{1}{2})^j F(-1) - (-\tfrac{1}{2})^j F(1) \right] \end{aligned}$$

Linearization of the integral flux term about a specified test solution V_0 gives

$$\mathbf{M} \frac{\partial \mathbf{V}}{\partial t} - \triangle x^{-1} \mathbf{A} \mathbf{V} = -\triangle x^{-1} (\mathbf{S} + \mathbf{F}_0 - \mathbf{A}\mathbf{V}_0) \tag{7}$$

where* $\mathbf{M} \equiv [m_{j,k}]$, $\mathbf{V} \equiv [v_j]$, $\mathbf{A} = \frac{\partial \mathbf{F}}{\partial \mathbf{V}}$, $\mathbf{F} \equiv [f_j]$, $\mathbf{S} \equiv [s_j]$,

$$m_{j,k} = \int_{-\frac{1}{2}}^{\frac{1}{2}} \xi^{j+k} \, d\xi, \qquad s_j = \begin{cases} 0 & \text{for } j \text{ even} \\ \frac{1}{2}^j & \text{for } j \text{ odd} \end{cases}$$

and

$$f_j = \int_{-\frac{1}{2}}^{\frac{1}{2}} j\xi^{j-1} F(V(\xi)) \, d\xi$$

Equation (7) is stable if the eigenvalues of $\mathbf{M}^{-1}\mathbf{A}$ lie in the left-hand plane, with one exception. Note that the first row of $\mathbf{A}$ is zero, which produces at least one zero eigenvalue. However, the equation for $j = 0$ is simply the constraint that the time rate of change of the average value of the solution depends only on the flux imbalance, which in this analysis is specified. Thus, this particular eigenvalue does not affect the stability of the system. To avoid confusion, we examine the eigenvalues of a modified matrix $\hat{\mathbf{A}}$ in which this zero eigenvalue has been eliminated. The modified equation is obtained by discarding the $j = 0$ equation and eliminating the v_0 component of the solution from the remaining equations by requiring that the average value of V be a specified constant.

Because equation (7) is nonlinear, the eigenvalues cannot be evaluated until the solution is known. However, the exact solution is not known and may not even exist. For the purposes of this analysis, the eigenvalues are evaluated by using a test solution V_0 that is obtained by projecting the initial solution onto the solution subspace $\mathcal{S}$. This test solution is given by

$$\int_{-\frac{1}{2}}^{\frac{1}{2}} \xi^j V_0(\xi) \, d\xi = \int_{-\frac{1}{2}}^{\xi_s} \xi^j d\xi - \int_{\xi_s}^{\frac{1}{2}} \xi^j d\xi \tag{8}$$

where $\xi_s = (X_s - \bar{x})/\triangle x$ is the location of the shock within the element in terms of element coordinates.

The $\hat{\mathbf{A}}$ and its eigenvalues σ are readily computed for any shock position within the element. Figures 1(a)-1(e) show the real part of the eigenvalues $\mathrm{Re}(\sigma)$ as a function of shock position for $n = 1$ through 5, respectively. In all cases, all eigenvalues are zero when the shock is on the boundary. For $n \leq 2$, all eigenvalues have a negative real part for $-\frac{1}{2} < \xi_s < \frac{1}{2}$. For $n > 2$, the real part of the eigenvalues becomes positive when the shock is close to the boundary of the element ($\xi_s \approx \pm\frac{1}{2}$); and hence, the method is unstable for these cases. This result is consistent with the numerical results of reference 1.

When V is a polynomial of degree n, then $F(V)$ is a polynomial of degree $2n$; however, the flux polynomial can be truncated to degree $n+1$ with no formal loss of accuracy. In reference 1, it was observed that the solution obtained with $n = 2$ was stable when the flux polynomial was evaluated exactly, and unstable when the flux polynomial was truncated. (Note that truncation of the flux is not an issue in the $n = 1$

*Matrix and vector indices range from 0 through n.

case because $n+1=2n$.) The eigenvalues shown in figures 1(a)-1(e) were computed using the exact flux (no truncation). Figure 2 shows the eigenvalues for $n=2$ in which the degree of the flux polynomial is truncated to $n+1=3$. In this case, the eigenvalues are positive for shock positions near the boundary. Again, the analysis agrees with the numerical results.

A physical understanding of why the element may become unstable can be obtained by looking at the test solution as the shock approaches the element boundary. Figures 3(a) and 3(b) illustrate typical solutions for $n=2$ and $n=3$, respectively. As the shock approaches the right boundary, the solution on that boundary becomes positive. As this occurs the physics within the element dictate the movement of "mass" into the neighboring element. However, the approximate Riemann fluxes that are commonly used do not allow the flux to switch until the average velocity on the element boundary becomes positive, and this change cannot take place until an overshoot has occurred (i.e., $V(\frac{1}{2})>1$).

Alternate Flux Formulas

If the conjecture described above is accurate, then the instability can perhaps be eliminated by changing the definition of the approximate Riemann flux such that it becomes dependent on the solution within the shocked element as the shock approaches the edge. For the purposes of this analysis, let the approximate Riemann flux at an element boundary be defined as the sum of all contributions that leave the elements on either side of the element boundary:

$$\begin{aligned}\mathcal{F}^R(U_L,U_R) &\equiv \max(0,U_L)U_L/2 \\ &+ \min(0,U_R)U_R/2 \end{aligned} \tag{9}$$

The equation for the element that contains a shock becomes

$$\begin{aligned}&\int_{-\frac{1}{2}}^{\frac{1}{2}} \xi^j \frac{\partial V}{\partial t}\, d\xi - \triangle x^{-1} \int_{-\frac{1}{2}}^{\frac{1}{2}} j\xi^{j-1} F(V)\, d\xi \\ &\quad + \triangle x^{-1}\left[s^+(\tfrac{1}{2})^j F(V(1/2)) \right. \\ &\quad \left. -s^-(-\tfrac{1}{2})^j F(V(-1/2))\right] \\ &\quad = -\triangle x^{-1}\left[(\tfrac{1}{2})^j F(-1) - (-\tfrac{1}{2})^j F(1)\right] \end{aligned} \tag{10}$$

where $s^\pm=1$ if $\pm V(\pm 1/2)>0$ and $s^\pm=0$ otherwise. When $s^\pm\neq 0$, the $j=0$ equation is not degenerate and the eigenvalues of the full matrix $\mathbf{A}$ must be considered. The eigenvalues of the $\mathbf{A}$ or $\hat{\mathbf{A}}$ matrices produced by the above set of equations are shown in figures 4(a)-4(e). Because the eigenvalues are unchanged when the shock position is not near the element boundary, these figures focus on a small region near $\xi_s=0.5$. The real part of the eigenvalues is positive for all shock positions for $n<4$. For $n=5$, one eigenvalue becomes positive in a small region near $\xi_s=0.487$ suggesting a possible instability.

The flux given in equation (9) is stable for $n<5$ and has most of the properties desired of a conservative flux: it is continuous, monotone, and $\mathcal{F}^R(U,U)=F(U)$. However, some concern exists regarding the property that $\mathcal{F}^R(U_L,U_R)$ can exceed both $F(U_L)$ and $F(U_R)$ in the region $U_L>0$, $U_R<0$. For example, when $U_L=-U_R=u$, then $\mathcal{F}^R(u,-u)=2F(u)$. This can be remedied either by limiting the flux or by taking an average of the contributions from the left and right elements (but only in regions were $U_L\cdot U_R<0$). Note that a limiter of the form $\mathcal{F}^R_{\rm lim}=\min(\mathcal{F}^R(U_L,U_R),F(U_L),F(U_R))$ does not affect the formal accuracy of the discontinuous Galerkin method. The average can be either a simple algebraic average or a weighted average that depends on the relative magnitudes of the characteristic speeds; however, the algebraic averaging results in a flux that is a discontinuous function of U_L and U_R.

Both limiting and weighted averaging causes the contribution of the flux to the shocked element to depend on the solutions in both the shocked element and the neighboring element. Consequently, an analysis of just the shocked element would be of questionable value. Such a case would require at least an analysis of two coupled elements; however, this analysis is left for future work. In the case with algebraic averaging, the degree to which the approximate Riemann flux contributes to the solution in the shocked element depends only on the solution within that element, and the current single-element analysis is still possible. The equations in the shocked element are similar to those given in equation (10) but with $s^\pm=1/2$ if $\pm V(\pm 1/2)>0$ and $s^\pm=0$ otherwise. (Note that the right-hand side also is different but does not enter into the analysis.) The eigenvalues for $n=2$ and 4 are shown in figures 5(a) and 5(b), respectively. Both cases are stable have eigenvalues and are similar to the non-averaged case. Similar results are found for values of $n<5$ while the $n=5$ case is still unstable.

Numerical Test

Numerical tests of the discontinuous Galerkin method with the modified approximate Riemann flux are presented in figures 6 and 7. The initial condition used for these tests is $U(x,0)=\bar{U}+\cos(2\pi x)$, where $\bar{U}$ is either 0 or 1/2. With this initial solution, a shock begins to form shortly after $t=0.15$. The

solution is evolved in time by using a third-order Runge-Kutta method, as described in reference 1.

Figure 6(a) shows the evolution of the solution up to $t = 0.4$ for $n = 3$ and with the domain partitioned into 20 uniformly spaced elements. Figure 6(b) shows solutions at $t = 0.4$ for $n = 0$ through 5. This grid resolution places the exact shock position on an element boundary. The solutions are smooth and stable for all values of n tested. Figure 6(c) shows a similar case with 22 elements which places the shock at the center of an element. For $n > 1$, the solutions have considerable oscillations that are not aesthetically pleasing, but the oscillations are bounded in time and are confined to the element that contains the shock and the elements on either side of that element. Furthermore, if the element average is plotted, as in figure 6(d), then the element-averaged solution is monotone in every case. Figures 7(a) and 7(b) show the moving shock case that results when $\bar{U} = 1/2$. Figure 7(a) shows the local solution for $t = 0.4$, $n = 0$ through 5, and figure 7(b) shows the local and element-averaged solution for $n = 3$. Again, the oscillations do not increase with n, the oscillations are confined to the neighborhood of the shock, and the element-averaged solution is quite well behaved. Tests that employed some form of averaging when $U_L \cdot U_R < 0$ showed no significant change in the solutions.

Euler Equations

In this section, the quadrature-free from of discontinuous Galerkin is applied to the Euler equations given by

$$U = \begin{bmatrix} \rho \\ \rho E \\ \rho u \end{bmatrix}, \qquad F = \begin{bmatrix} \rho u \\ u(\rho E + P) \\ \rho u^2 + P \end{bmatrix}$$

where $P = (\gamma - 1)(\rho E - \frac{1}{2}\rho u^2)$.

The first requirement for the implementation of the quadrature-free form of discontinuous Galerkin is that the flux must be written as a polynomial. But unlike Burgers' equation, an exact polynomial form for the Euler flux does not exist. When rewritten in terms of the dependent variables ρ, ρE, and ρu, the flux involves the terms

$$f_1 = \frac{(\rho u)(\rho E)}{\rho}, \quad f_2 = \frac{(\rho u)^2}{\rho}, \quad f_3 = \frac{(\rho u)^3}{\rho^2}$$

Polynomial approximations of the form

$$f_i = \sum_0^{n+1} \xi^k f_{i,k}$$

are obtained by projection by solving

$$\int_{-1/2}^{1/2} \xi^j \rho f_i \, d\xi = \int_{-1/2}^{1/2} \xi^j R_i \, d\xi$$

for $j = 0, 1, \ldots, n+1$, where $R_i = (\rho u)(\rho E)$, $(\rho u)^2$, and $(\rho u) f_2$ for $i = 1$, 2, and 3, respectively. The equations are linear in the unknowns $f_{i,k}$, and each equation set has the same matrix on the left-hand side of the equation.

For initial tests, the approximate Riemann flux is obtained by splitting F according to the sign of the eigenvalues of the Jacobian of F. Thus, if

$$F = AU = L\,[\lambda]\,L^{-1}U$$

then

$$\begin{aligned} \mathcal{F}(U_L, U_R) &= \left(L\,[\lambda^+]\,L^{-1}\right)_{U_L} U_L \\ &+ \left(L\,[\lambda^-]\,L^{-1}\right)_{U_R} U_R \\ &\equiv F^+(U_L) + F^-(U_R) \end{aligned}$$

The test problem is periodic on the domain $0 < x < 1$ with initial conditions

$$\begin{aligned} &\rho = 1 + 0.1\,\sin(2\pi x) \\ &P = \rho^\gamma, \qquad a = \sqrt{\gamma P/\rho} \\ &u = u_\infty \pm \tfrac{2}{\gamma - 1}(a - \sqrt{\gamma}) \\ &\rho E = P/(\gamma - 1) + \rho u^2/2 \end{aligned}$$

that produce a single isentropic acoustic wave that propagates at an average speed of $u_\infty \pm \sqrt{\gamma}$. The initial discrete solution is obtained by fitting a polynomial through the exact initial solution at the Chebyshev-Gauss-Lobatto points within each element.

The acoustic wave propagates in the $\pm\xi$-direction (relative to u_∞), steepens to form a shock, and then gradually decays in time. Figures 8(a) and 8(b) show solutions at $t = 3$ for right-traveling waves with $u_\infty = 2.0\sqrt{\gamma}$ and $0.5\sqrt{\gamma}$, respectively. At these values for u_∞, each eigenvalue of the Jacobian A is of a constant sign throughout the domain. Thus, the functional form of the flux is the same everywhere, and the situation in which $\lambda_{U_L} > 0$ and $\lambda_{U_R} < 0$ does not occur for any eigenvalue. As in the results with Burgers' equation, the solution is stable, the oscillations are confined to the neighborhood of the shock, and they remain roughly the same magnitude as the formal order of the method n is increased.

With $u_\infty = -\sqrt{\gamma}$, the shock is stationary, and the sign of the eigenvalue associated with the right-traveling wave changes across the shock. As shown

in figure 9, the solutions are considerably more oscillatory in this case, and a distinct difference is evident between solutions obtained with odd and even values of n. In the region on the left side of the shock, the oscillations do not grow as n is increased, but they are not confined to the shock region as in the moving-shock case. In the region on the right side of the shock, results with odd values of n are smooth, but results with even values of n are highly oscillatory. The reasons for this unusual dependence on n is not known at this time. Results obtained with this simple flux are stable but lack sufficient accuracy, and further work is needed.

The appearance of the solution can be improved either by adding dissipation or by applying a filter to the solution at each time step. Efforts to develop high-order dissipation terms have not been successful thus far; however, filters that are both compact and robust have been developed. The filter has the form $\mathbf{V} = \mathbf{T}^{-1}\mathbf{d}\mathbf{T}\mathbf{V}$, where $\mathbf{T}$ is the constant matrix that relates the coefficients of a general polynomial to the coefficients of an equivalent Legendre expansion. The diagonal matrix $\mathbf{d} = (\epsilon_0, \epsilon_1, \ldots, \epsilon_m, \ldots)$ contains the damping coefficients. Figure 10 shows results with $\epsilon_i = \epsilon^i$ for several constant values of ϵ. This filter is capable of removing oscillations; however, the accuracy is reduced to first order for smooth flows. Development of high-order filters and adaptive filters may be required.

Concluding Remarks

An analysis is presented of the discontinuous Galerkin method for a scalar nonlinear model problem that contains a shock. The transition from a stable to an unstable method as the degree of the method is increased from 2 to 3 is correctly predicted by the analysis. Also, the instability associated with truncating the flux polynomial is also predicted. Insight gained from the analysis suggests a possible source for the instability and leads to a modified approximate Riemann flux that eliminates the instability. The elimination of the instability is predicted in the analysis of the modified method and is verified by numerical experiment using Burgers' equation. Although the solutions are oscillatory in the neighborhood of the shock, the oscillations are bounded and are confined to the neighborhood of the shock. Furthermore, the element-averaged solution is monotone, which suggests that a smooth solution can be obtained by applying a filter as a post processing step. Numerical experiments with the Euler equations showed that the modified approximate Riemann flux resulted in a stable scheme. Cases in which the shock was in motion such that eigenvalues did not change sign across the shock produced results similar to those observed with Burgers' equation. In other cases, however, the oscillations were not confined to the shock region, and some type of filtering is necessary.

References

1. H. L. Atkins and Chi-Wang Shu, "Quadrature-free implementation of the discontinuous Galerkin method for hyperbolic equations," AIAA paper no. 96-1683, 1996.

2. H. L. Atkins and Chi-Wang Shu, "Continued development of the discontinuous Galerkin method for aeroacoustic applications," AIAA paper no. 97-1581, 1997.

3. B. Cockburn and C.-W. Shu, "TVB Runge-Kutta local projection discontinuous Galerkin finite element method for conservation laws II: General framework," *Mathematics of Computation*, v52 (1989), pp. 411-435.

4. B. Cockburn, S. Y. Lin, and C.-W. Shu, "TVB Runge-Kutta local projection discontinuous Galerkin finite element method for conservation laws III: One dimensional systems," *Journal of Computational Physics*, v84 (1989), pp. 90-113.

5. B. Cockburn, S. Hou, and C.-W. Shu, "The Runge-Kutta local projection of discontinuous Galerkin finite element method for conservation laws IV: Multidimensional case," *Mathematics of Computation*, v54 (1990), pp. 545-581.

6. G. Jiang and C.-W. Shu "On cell entropy inequality for discontinuous Galerkin methods," *Mathematics of Computation*, v62 (1994), pp. 531-538.

7. R. B. Lowrie, P. L. Roe, and B. van Leer, "A space-time discontinuous Galerkin method for time-accurate numerical solution of hyperbolic conservation laws," AIAA paper no. 95-1658, 1995.

8. P. L. Roe, "Some contributions to modeling discontinuous flows," in *Large Scale Computations in Fluid Mechanics*, Lectures in Appl. Math., Vol. 22-2, (Amer. Math. Soc., Providence, RI, 1985).

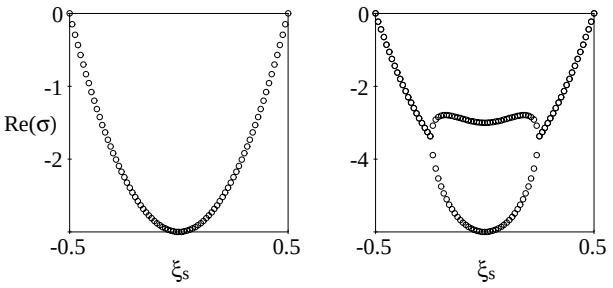

a) $n = 1$. b) $n = 2$.

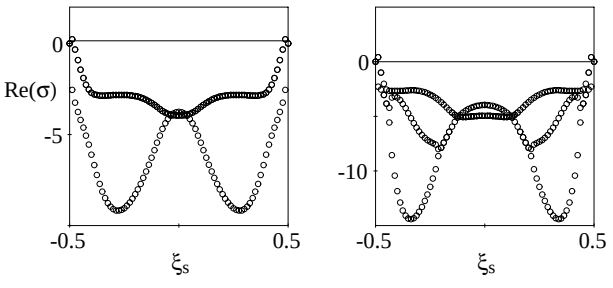

c) $n = 3$. d) $n = 4$.

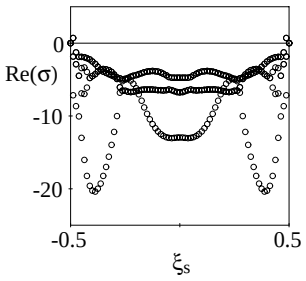

e) $n = 5$.

Figure 1. Real part of eigenvalues of baseline discontinuous Galerkin method.

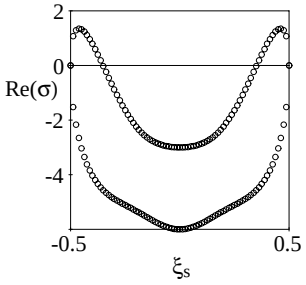

Figure 2. Real part of eigenvalues for $n = 2$ with flux polynomial truncated to $n + 1 = 3$.

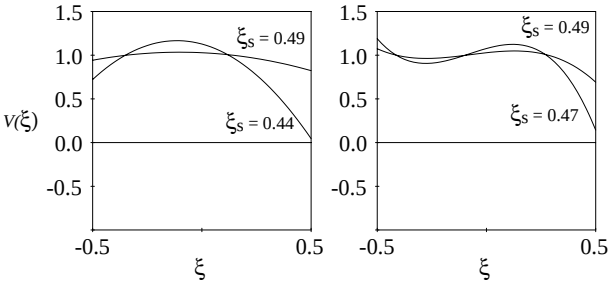

a) $n = 2$. b) $n = 3$.

Figure 3. Test solution when shock is near right boundary.

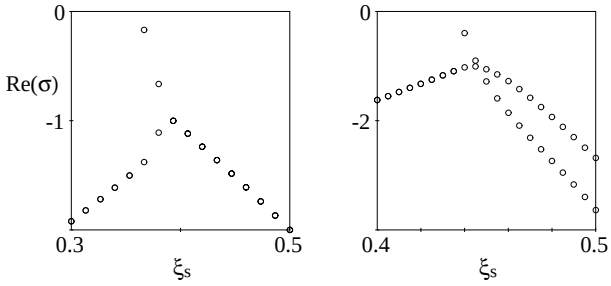

a) $n = 1$. b) $n = 2$.

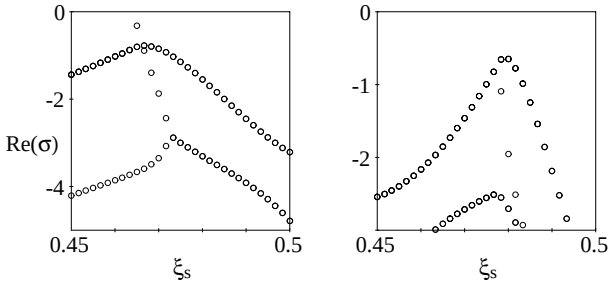

c) $n = 3$. d) $n = 4$.

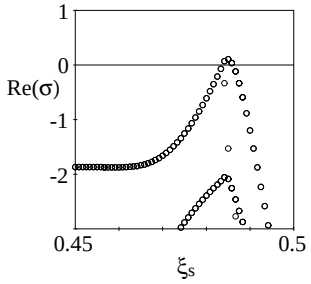

e) $n = 5$.

Figure 4. Real part of eigenvalues of discontinuous Galerkin method with Riemann flux given by equation (9).

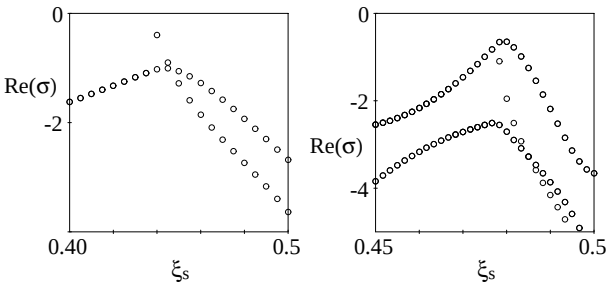

a) $n = 2$. b) $n = 4$.

Figure 5. Real part of eigenvalues with averaging used in Riemann flux.

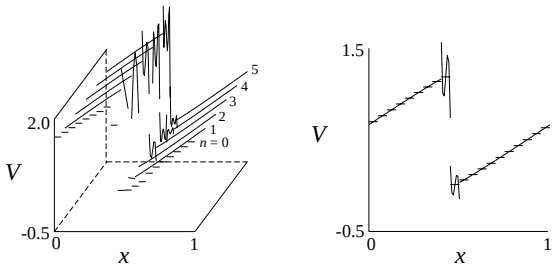

a) Local solution, $n = 0$–5, $t = 0.4$.

b) Local and element-averaged solution for $n = 3$, $t = 0.4$.

Figure 7. Numerical solution with modified Riemann flux for moving shock.

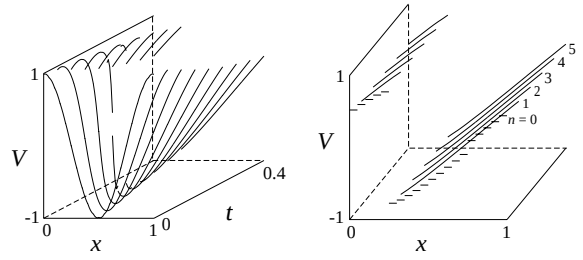

a) Evolution of solution with shock at element boundary: $n = 3$.

b) Shock at element boundary: $n = 0$–5, $t = 0.4$.

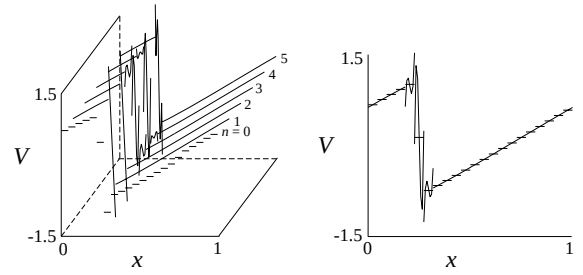

c) Shock at mid-element: $n = 0$–5, $t = 0.4$.

d) Local and element-averaged solution with shock at mid-element: $n = 3, t = 0.4$.

Figure 6. Numerical solution with modified Riemann flux for stationary shock.

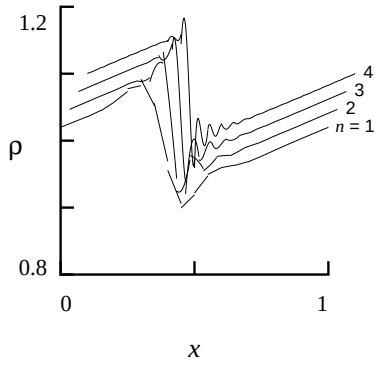

a) $u_\infty = 2.0\sqrt{\gamma}$.

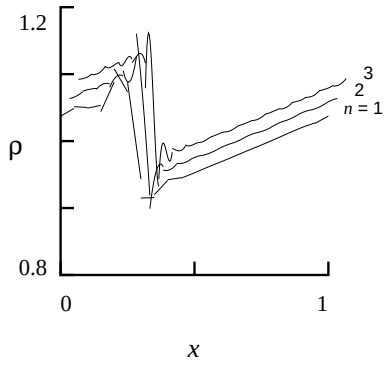

b) $u_\infty = 0.5\sqrt{\gamma}$.

Figure 8. Solution to Euler equations at $t = 3$ with u_∞ chosen such that flux splitting is essentially fixed.

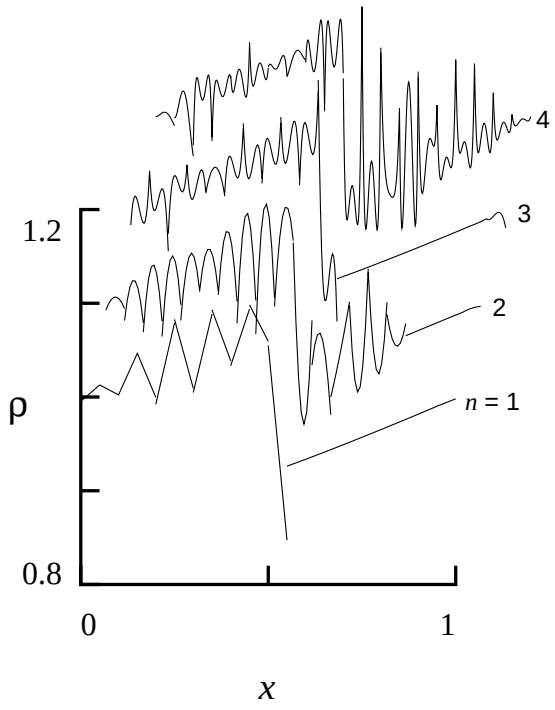

Figure 9. Solution to Euler equations at $t = 3$ with $u_\infty = -\sqrt{\gamma}$.

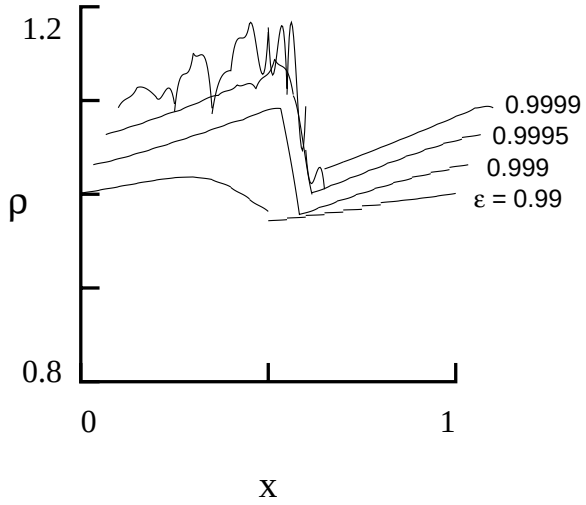

Figure 10. Solution to Euler equations at $t = 3$ with $u_\infty = -\sqrt{\gamma}$ and $n = 3$ with spectral filter.